Journal of Alloys and Compounds 509 (2011) 3393–3397

Contents lists available at ScienceDirect

Journal of Alloys and Compounds

journal homepage: www.elsevier.com/locate/jallcom

Structural and microwave absorption properties of $Ni_{(1-x)}Co_{(x)}Fe_2O_4$ ($0.0 \leq x \leq 0.5$) nanoferrites synthesized via co-precipitation route

Asghari Maqsood*, Kishwar Khan

Thermal Transport Laboratory, School of Chemical and Materials Engineering (SCME), National University of Sciences and Technology (NUST), H-12 Islamabad, Pakistan

ARTICLE INFO

Article history:
Received 20 August 2010
Received in revised form 9 December 2010
Accepted 10 December 2010
Available online 21 December 2010

Keywords:
NiCo nanoparticles
Synthesis
Microwave absorbing properties

ABSTRACT

Ni–Co nanoferrites show excellent magneto-dielectric properties and these materials can be used to miniaturize the size of the high frequency devices which is the order of the day. Nanocrystalline Ni–Co ferrites having general formula $Ni_{1-x}Co_xFe_2O_4$ ($x = 0.0$, 0.1, 0.2, 0.3, 0.4, and 0.5) were prepared by co-precipitation method. The structural morphology of the prepared samples was carried out using scanning electron microscopy. The results showed the spherical shaped nanoparticles varying in the range of 16–40 nm. The complex relative permittivity (ε_r) and complex relative permeability (μ_r) were measured using vector network analyzer for all the samples in the frequency range of 1 MHz to 3 GHz. The variation of complex relative permittivity (ε_r) as a function of frequency is explained in accordance with Maxwell–Wagner model and Koop's phenomenological theory. The effect of frequency and cobalt concentration on permeability are reported. The reflectivity (R) of nanoferrites is also calculated. The value of minimum reflection loss (RL) is about −18 dB at 2.45 GHz with a thickness of 2.1 ± 0.1 mm. The results indicate that $Ni_{1-x}Co_xFe_2O_4$ nanoparticles have excellent microwave absorbing properties and have a great potential for military use.

1. Introduction

Ferrite is one of the materials used for an electromagnetic wave absorber [1]. A number of investigations have been reported for studying the effect of composition on the electromagnetic wave absorption properties [2]. The microstructure and magnetic properties of polycrystalline ferrites are highly sensitive to the preparation techniques, doping level and the sintering conditions [3,4].

The spinel ferrites show interesting magnetic and electrical properties in the nano crystalline form compared with those of the micrometer-size grains. Nano-phase spinel ferrites have attracted much attention due to their technological importance in different fields, such as microwave devices, high speed digital tapes and disk recording, ferro-fluids, catalysis, and magnetic refrigeration systems [5–7], biosensors, recording colour imaging, targeted drug delivery, catalysts, and pigments [8,9]. The interesting and useful magnetic properties of spinel ferrites depend on the choice of cations along with Fe^{2+} and Fe^{3+} ions and their distribution between tetrahedral (A) and octahedral (B) sites of the spinel lattice [4,10–12].

Ni–Co ferrites are important electronic materials which are used in electronic devices suited for high-frequency applications in the telecommunication field [12]. These materials are commercially used in high-quality filters, rod antenna radio frequency circuits, transformer cores, read/write heads for high-speed digital tape and operating devices [12,13]. The excellent electromagnetic properties of these materials make them suitable for size reduction of high frequency application devices. The size of the antenna can be reduced using a material of higher refractive index, i.e. $n = (\varepsilon' \cdot \mu')^{1/2}$ where n is the refractive index, ε' and μ' are the real values of permittivity and permeability, respectively [14]. In the present work, the permittivity and permeability of the synthesized Ni–Co ferrites prepared by co-precipitation method is reported in the frequency range of 1 MHz to 1 GHz to find their usefulness in high frequency devices. The preparation detail and characterization of this material by X-ray and electrical properties are described elsewhere [15]. The lattice constants and particle size obtained from X-ray data are given in Table 1.

2. Experimental procedures

2.1. SEM and EDS studies

Scanning electron microscopy images (SEM) and EDX were made using a JEOL-instrument Japan (JSM-3-5-CF). SEM micrographs of co-precipitated Ni-ferrites and their partial distribution are shown in Fig. 1. As seen from the micrographs, the dimension of the particle is varying in the range of 16–40 nm.

* Corresponding author. Tel.: +92 51 90855203; fax: +92 51 8318499.
E-mail addresses: tpl.qau@usa.net (A. Maqsood), kishwar.nust@gmail.com (K. Khan).

0925-8388/$ – see front matter © 2010 Elsevier B.V. All rights reserved.
doi:10.1016/j.jallcom.2010.12.082

Table 1
Crystallite size t for (3 1 1), real and imaginary parts (ε', ε'') of the permittivity at 1 GHz and 3 GHz. For XRD see Ref. [7].

Parameters	Cobalt concentration					
	$x=0.0$	$x=0.1$	$x=0.2$	$x=0.3$	$x=0.4$	$x=0.5$
$t_{(311)}$ nm	17	21	15	25	23	33
ε'at 1 GHz	3.44	3.23	3.22	2.99	2.04	1.34
ε' at 3 GHz	12.60	12.30	11.20	11.10	7.14	4.88
ε'' at 1 GHz	10.20	15.80	17.70	28.9	60.40	75.40
ε'' at 3 GHz	11.40	11.8	12.00	12.20	41.60	66.00
tan δ at 1 GHz	0.0212	0.0297	0.0869	0.0530	0.0866	0.0563
tan δ at 3 GHz	1.02	0.940	0.925	0.928	0.918	0.953

2.2. Magneto-dielectric measurements

The complex permittivity and permeability of the samples have been measured using an Agilent E4991A RF impedance/materials analyzer [16] over 1 MHz to 1 GHz, with the 16453A (permittivity) and 16454A (permeability) test fixtures, respectively.

The capacitance method was used to measure relative permittivity. The dielectric constant (ε_r) was calculated by the standard relation [17].

$$\varepsilon_r = \frac{Cd}{\varepsilon_0 A} \tag{1}$$

where C is the capacitance of the pellet in farad, d is the thickness of the pellet in meters, A is the cross-sectional area of the flat surface of the pellet and ε_0 is the permittivity for free space.

The dielectric loss tangent (D_ε) for a sample was measured directly, which could be determined in terms of real (ε') and imaginary parts (ε'') of dielectric constant as

$$\mathrm{D}_\varepsilon = \tan\delta = \frac{\varepsilon''}{\varepsilon'} \tag{2}$$

The E4991A uses the inductance method to measure relative permeability. In this method, a DUT (toroidal core) is wrapped with a wire, and the relative permeability is calculated from the inductance values at the end of the core.

The complex relative permeability of the ring sample can be determined by the relation

$$\mu_r = \frac{2\pi(L - L_s)}{\mu_0 h \ \ln(c/b)} + 1 \tag{3}$$

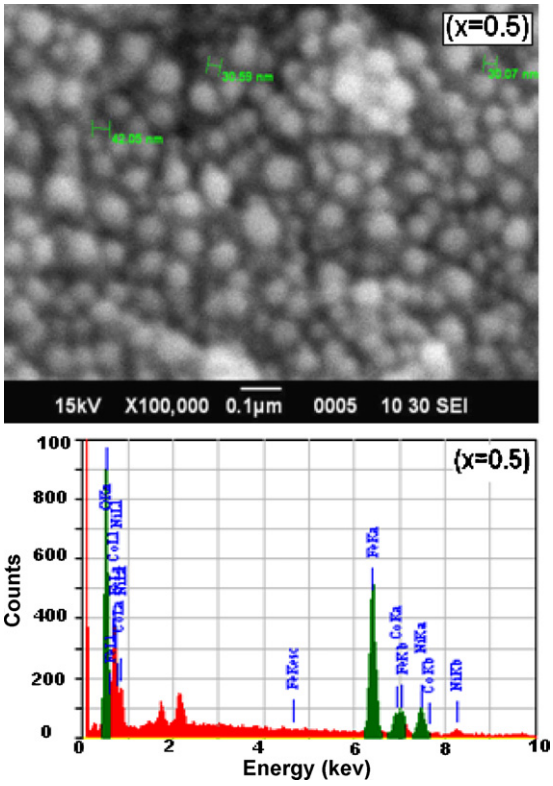

Fig. 1. SEM and EDX of sintered powders of $Ni_{(1-x)}Co_{(x)}Fe_2O_4$ at 800 °C for 8 h.

Table 2
Lattice constants a_{exp} obtained from XRD, real and imaginary parts of the complex relative permeability and reflectivity (R) at 1 GHz and 3 GHz.

Parameters	Cobalt concentration					
	$x=0.0$	$x=0.1$	$x=0.2$	$x=0.3$	$x=0.4$	$x=0.5$
a_{exp} (A)	8.335	8.341	8.342	8.344	8.345	8.346
SEM (nm)	45	25	20	16	24	30
μ' at 1 GHz	384.63	450.65	382.02	303.32	357.80	235.04
μ'' at 1 GHz	18.20	21.40	17.00	15.60	14.40	11.10
R (dB) at 1 GHz	−1.60	−1.53	−1.76	−1.74	−1.63	−1.07
R (dB) at 3 GHz	−2.99	−2.93	−3.40	−3.36	−3.05	−2.03

where L is the inductance of 16454A test fixture with sample and L_s is the inductance of the same test fixture without sample, μ_0 is the relative permeability of air, h, b and c are the thickness, internal and outer diameters of the ring shaped sample. The inductance of 16453A test fixture is L_s calculated using the following relation [16]

$$L_s = \frac{\mu_0}{2\pi} h_0 \ \ln\frac{e}{a} \tag{4}$$

where h_0, e and a are the thickness, outer and internal diameters of the 16454A test fixture.

The magnetic loss tangent (D_μ) is determined by the relation

$$\mathrm{D}_\mu = \tan\delta = \frac{\mu''}{\mu'} \tag{5}$$

where $\mu'$and μ'' are the imaginary and real parts of the complex relative permeability, respectively.

The reflectivity (R) of nanoferrites is also calculated using the following formula [16]:

$$Z_{in} = \left[\frac{\mu_r}{\varepsilon_r}\right]^{1/2} \ \tanh\left[j\left(\frac{2\pi fd}{c}\right)(\mu_r\varepsilon_r)\right]^{1/2} \tag{6}$$

$$R(\mathrm{dB}) = 20 \ \log_{10}\left[\frac{Z_{in}-1}{Z_{in}+1}\right] \tag{7}$$

where Z_{in} is the normalized input impedance in free space, c is the velocity of light in vacuum, and f is the frequency of microwave in free space. $\varepsilon_r = (\varepsilon' - j\varepsilon'')$, $\mu_r = (\mu' - j\mu'')$, and d are the complex permittivity, complex permeability, and thickness of the sample, respectively.

3. Results and discussion

3.1. SEM morphology

SEM micrographs of $Ni_{1-x}Co_xFe_2O_4$ ($0.0 \le x \le 0.5$) nanoferrites are shown in Fig. 1. As seen from the micrographs, the dimension of the particle is varying in the range of 16–40 nm. Fig. 1 shows the surface morphology of $Ni_{(1-x)}Co_{(x)}Fe_2O_4$ samples with x ($0.0 \le x \le 0.5$), respectively. Relatively less porous, dense material formation is apparent in the samples with a remarkable change in grain size. The average grain size determined by the linear intercept method is fairly consistent with that obtained from XRD technique, already reported [15]. The EDS also shows a fair resemblance with initial composition. The comparison of the results of XRD (Table 1) and SEM reveals that, the substitution of Co ions for Ni in the $Ni_{1-x}Co_xFe_2O_4$ ferrite system shows an increase in bulk density and decrease in porosity and particle size of the host material. Similar observations are reported [17] (Table 2).

3.2. Complex relative permittivity

The frequency dependence of the dielectric constant for all the samples in the frequency range of 1 MHz to 1 GHz is shown in Fig. 2. A study of the figure shows that dielectric constant reached nearly a constant at higher frequency. After certain increase in frequency all the samples exhibit a nearly frequency independent behavior. The observed variation in ε' can be explained on the basis of space-charge polarization. According to Maxwell–Wagner two-layer model [18,19], the space-charge polarization is due to the inhomogeneous structure of dielectric material. It is formed by

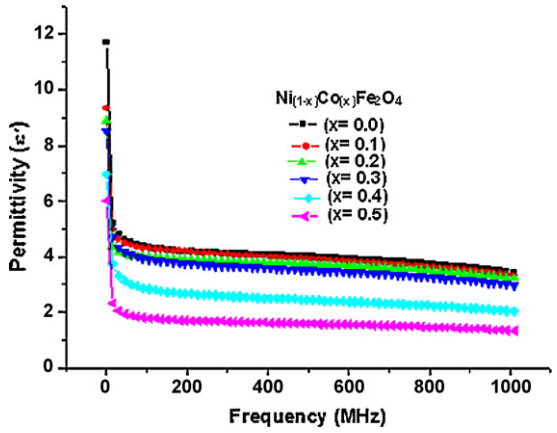

Fig. 2. Real permittivity of Ni–Co nanoferrites in the frequency range of 1 MHz to 1000 MHz.

large well conducting grains separated by poorly conducting grain boundaries [20]. The electrons reach the grain boundary through hopping. If the resistance of the grain boundary is large, the electrons pile up at the grain boundary and produce polarization. When the frequency of the applied field is increased, the probability of the electrons to reach the grain boundary decreases. This decreases the polarization and hence the dielectric constant decreases with increase in frequency [21,22].

Fig. 2 indicates that the dielectric constant also depend upon the increase of cobalt concentration in nickel ferrite. Iwauchi [23] pointed out that there is strong correlation between dielectric behavior and the conduction mechanism in ferrites. Conduction mechanism in Ni–Co ferrites is the result of electron and hole hopping between ions of same element exiting in different valence state on octahedral site [5,24]. Fe^{3+} ions distribute in two distinct sites, but most Fe^{3+} ions exist in octahedral site (B-site). The cobalt ferrite is known as the completely inverse spinel [25], while the nickel ferrite is mixed spinel structure with 80 degree of inversion. Therefore the increase in concentration of cobalt will result in replacement of Ni ions on A and B sites, as well as migration of Fe ions from B site to A site. The decrease in Fe ion on B site will result a decrease in electron hopping. As a result, less number of electrons reach the grain boundary, hence the polarization as well as the dielectric constant of the prepared samples decreased with increase in cobalt concentration.

Moreover, the nearest distance pairs of Fe^{2+}–Fe^{3+} decreased in B-sites with the increase of cobalt ions which tend to occupy octahedral sites. It resulted in the electron hopping between Fe^{2+} and Fe^{3+} ions and hole hopping Co^{3+} and Co^{2+} ions happen to longer distance in B-sites [26,27].

The graph of dielectric loss tangent with frequency is depicted in Fig. 3. Again the dielectric loss tangent decreased with increase in frequency for all samples. All the samples exhibit dispersion due

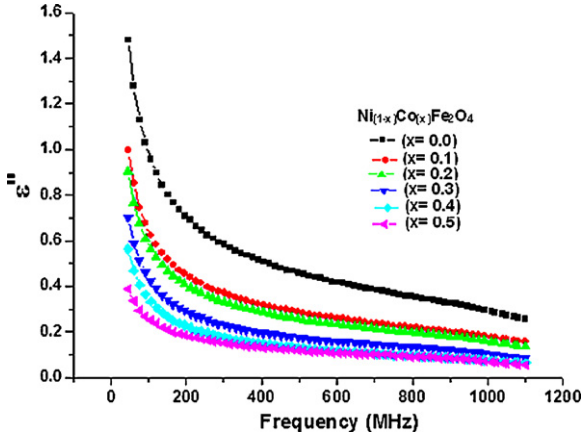

Fig. 3. Imaginary part of permittivity of Ni–Co nanoferrites in the frequency range of 1 MHz to 1000 MHz.

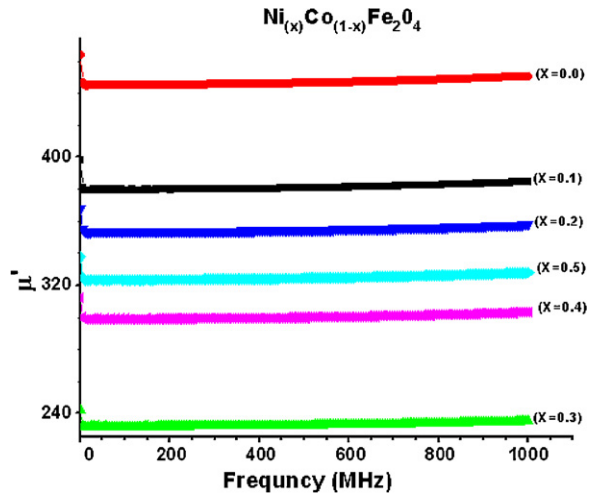

Fig. 4. Real part of permeability of Ni–Co nanoferrites in the frequency range of 1 MHz to 1000 MHz.

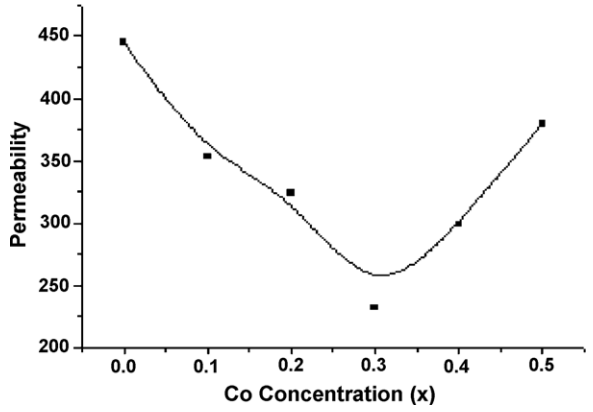

Fig. 5. Variation of permeability of Ni–Co ferrites as a function of Co concentration at 100 MHz.

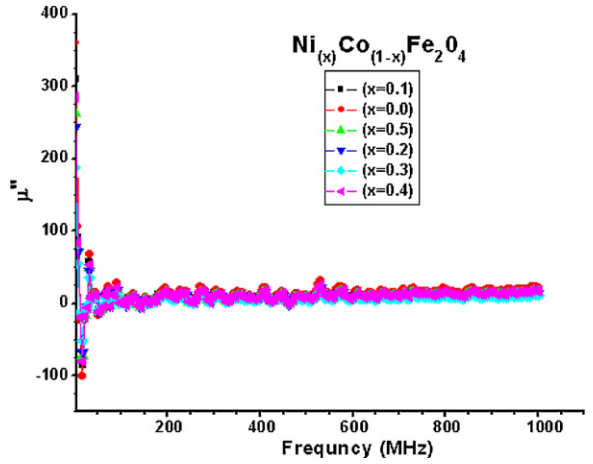

Fig. 6. Imaginary part of permeability of Ni–Co nanoferrites in the frequency range of 1 MHz to 1000 MHz.

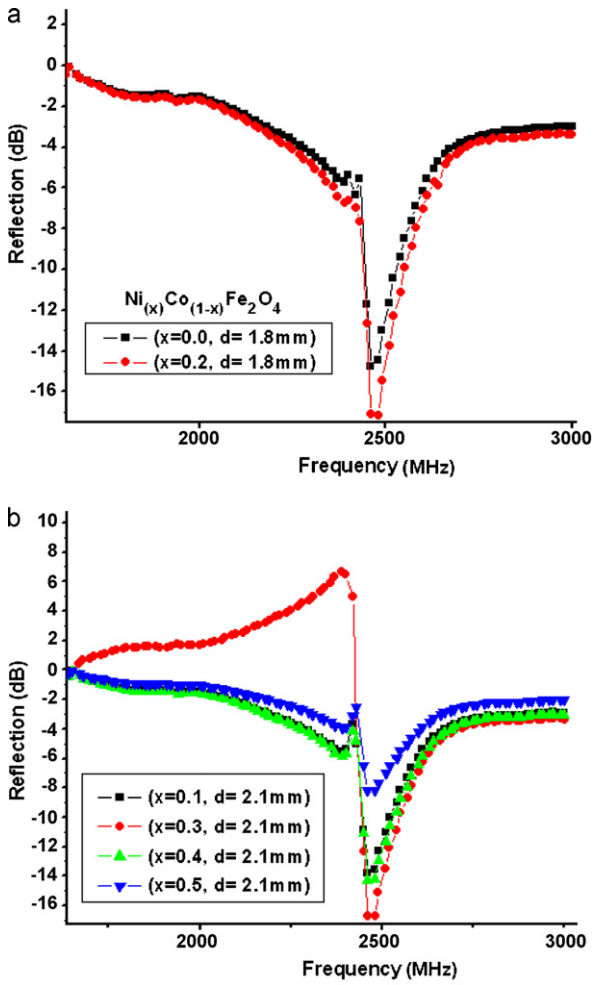

Fig. 7. (a) Microwave absorption curves of $x = 0.0$, $x = 0.2$ with thickness 1.8 ± 0.1 mm. (b) Microwave absorption curves of $x = 0.1$, $x = 0.3$, $x = 0.4$, and $x = 0.5$ with thickness of 2.1 ± 0.1 mm.

to Maxwell–Wagner interfacial type polarization and Koop's phenomenological theory [18–20]. The dielectric loss tangent of the prepared samples showed a decrease with increase in cobalt concentration. For the present case, the decrease in conductivity of the samples with increase in cobalt concentration resulted in decrease in dielectric losses.

3.3. Complex relative permeability

Complex relative permeability of all the prepared samples measured in the frequency range of 1 MHz to 1 GHz at room temperature is shown in Fig. 4. The permeability spectra of all the samples exhibited a common feature. The real permeability remains almost constant in the frequency range of 1 MHz to 1 GHz. Fig. 5 shows the composition dependence of permeability of the prepared samples. The permeability initially decreased with increase in cobalt concentration, attained the minimum value for the sample having $x = 0.3$ and then increased for the rest of the samples. The increase in concentration of cobalt will result in replacement of Ni ions on A and B sites, as well as migration of Fe ions from B site to A site. The initial decrease in permeability is due to migration of Fe ion from octahedral site to tetrahedral site. As the magnetic moment of Fe is larger as compared to that of Co and Ni ions, so the cancellation of net magnetization of A sublattice to B sub-lattice resulted in decrease of flux density as well as permeability of the prepared samples. Similar observations are reported by Watawe et al. [28]. The magnetic loss tangents of all the samples in the frequency range of 1 MHz to 1 GHz are shown in Fig. 6. The magnetic losses remained almost same in the measured frequency band.

3.4. Reflectivity (R)

Fig. 7(a) shows the reflectivity (R) values of with nearly same thickness ($\approx 1.8 \pm 0.1$ mm). According to the maximum absorption peak of the nanoferrites with ($x = 0.3$) in $Ni_{1-x}Co_xFe_2O_4$ is -18 at 2.45 GHz. When the concentration of cobalt was increased up to 0.3, the value of (R) becomes maximum, further increase in cobalt concentration gradually decreased the reflectivity (R). Fig. 7(b) also indicates that the composition of nanoferrites has no effect on the position of maximum absorbing peak but does affect the magnitude of the peak. In other words, the prepared samples exhibit good absorption performance in the 2–3 GHz frequencies and appear to be a potential microwave absorbing material [29].

4. Conclusions

Co-doped spinel-ferrites $Ni_{1-x}Co_xFe_2O_4$ nanoparticles with an average diameter of 16–40 nm were successfully prepared by co-precipitation method. The dielectric and microwave absorbing properties of the products were investigated in Ku-band. Both complex relative permittivity and complex relative permeability of the prepared samples showed the strong correlation with the structure. The frequency response of permittivity of Ni–Co nanoparticles can be explained on the basis of Maxwell–Wagner model and Koop's phenomenological theory. Thus Ni–Co nanoparticles showed a good absorption performance in the range of 2–3 GHz.

Acknowledgements

The authors specially acknowledge Dr. Muhktar Alum (Director Research & Planning) and Miss Syeda Nasiha Semi (Research Scholar) Plant Sciences Department, Hazara University Mansehra (KPK) for their moral support. The financial support of Pakistan Science Foundation (PSF) through project no. 147 is also acknowledged.

References

[1] S.G. Doh, E.B. Kim, B.H. Lee, J.H. Oh, J. Magn. Mater. 272 (2004) 2238.
[2] P. Singh, V.K. Babber, A. Razdan, S.L. Strivastava, T.C. Goel, Mater. Sci. Eng. B 78 (2000) 70.
[3] M.K. Shobana, S. Sanker, J. Magn. Magn. Mater. 321 (2009) 2125–2128.
[4] M. Ajmal, N.A. Shah, A. Maqsood, M.S. Awan, M. Arif, J. Alloys Compd. 508 (2010) 226–232.
[5] P.A. Shaikha, R.C. Kambalea, A.V. Raoa, Y.D. Kolekar, J. Alloys Compd. 492 (2010) 590.
[6] S.J. Shukla, K.M. Jadhav, G.K. Bichile, J. Pure Appl. Phys. 39 (2001) 226.
[7] M.I. Rosales, E. Amano, M.P. Cuautle, R. Valenzuela, Mater. Sci. Eng. B 49 (1997) 221.
[8] P.P. Sarangi, B.D. Naik, S.R. Vadera, M.K. Patra, C. Prakash, N.N. Ghosh, Mater. Technol. Adv. Perform. Mater. 24 (2009) 97–99.
[9] C. Scherer, A.M.F. Neto, Braz. J. Phys. 35 (2005) 718–727.
[10] I.H. Gul, A. Maqsood, M. Naeem, M.N. Ashiq, J. Alloys Compd. 507 (2010) 201–206.
[11] I.H. Gul, A. Maqsood, J. Alloys Compd. 465 (2008) 227.
[12] K. Karthik, G.H. Selvan, M. Kanagaraj, S. Arumug, M.N.V. Jaya, J. Alloys Compd. 509 (2011) 181–184.
[13] S. Rehman, A. Mumtaz, S.K. Hasanain, J. Nanopart. Res. (2010), doi:10.1007/s11051-010-11143-8.
[14] L.B Kong, Z.W. Li, G.Q. Lin, Y.B. Gan, Acta Mater. 55 (2007) 6561–6572.
[15] A. Maqsood, K. Khan, M.A. Rehman, M.A. Malik, J. Supercond. Nov. Magn. (2010), doi:10.1007/s10948-010-0956-9.
[16] Agilent Technologies. "Theory on material measurement, operational manual E" Agilent Part No. E4991-90070 (2005).
[17] M. Naeem, N.A. Shah, I.H. Gul, A. Maqsood, J. Alloys Compd. 487 (2009) 739–743.
[18] J.C. Maxwell, Electricity and Magnetism, vol. 1, Oxford University Press, Oxford, 1929, p. 328.
[19] K.W. Wagner, Ann. Phys. 40 (1913) 817.
[20] C.G. Koops, Phys. Rev. 83 (1951) 121.

[21] A.K. Singh, T.C. Goel, R.G. Mendiratta, J. Appl. Phys. 91 (2002) 6626.
[22] M. Ajmal, A. Maqsood, Mater. Lett. 62 (2008) 2077.
[23] K.J. Iwauchi, Appl. Phys. 10 (1971) 1520.
[24] E.J.W. Verwey, E.L. Heilman, J. Chem. Phys. 15 (1947) 174.
[25] E. Mendelovici, R. Vilalba, A. Sagarazu, Thermochim. Acta 318 (1998) 51–56.
[26] P.F. Bernath, J.H. Black, J.W. Brault, J. Astrophys. 298 (1985) 375.
[27] A. Lakshman, P.S. Rao, B.P. Rao, K.H. Rao, J. Phys. D: Appl. Phys. 38 (2005) 673.
[28] S.C. Watawe, B.D. Sarwade, S.S. Bellad, B.D. Sutar, B.K. Changule, Mater. Chem. Phys. 65 (2000) 173.
[29] J. de los Santos, D. Garcia, J. A. Eiras, Mater.Res., doi:10.1590/s1516-14392003000100017.